Zhang et al. *Zool. Res.* 2025, 46(6): 1273−1288
https://doi.org/10.24272/j.issn.2095-8137.2025.031
https://cstr.cn/32248.14.zr.2025.031

ZR | Zoological Research

Article Open Access

Maternal hypoxia exposure perturbs imprinted gene methylation in adult sperm and induces intergenerational placental impairments in male offspring

Lu-Yao Zhang[1,3,#], Gong-Xue Jia[1,3,#], Hai-Ping Tao[1,3], Ke-Xiong Liu[5], Yu-Wen Luo[2], Yun-Peng Hou[2,*], Qi-En Yang[1,3,4,*]

[1] *Key Laboratory of Adaptation and Evolution of Plateau Biota*, *Northwest Institute of Plateau Biology*, *Chinese Academy of Sciences*, *Xining*, *Qinghai* 810001, *China*

[2] *State Key Laboratory of Animal Biotech Breeding*, *College of Biological Sciences*, *China Agricultural University*, *Beijing* 100193, *China*

[3] *University of Chinese Academy of Sciences*, *Beijing* 100049, *China*

[4] *Qinghai Key Laboratory of Animal Ecological Genomics*, *Northwest Institute of Plateau Biology*, *Chinese Academy of Sciences*, *Xining*, *Qinghai* 810008, *China*

[5] *Institute of Animal Husbandry and Veterinary Medicine*, *Beijing Academy of Agriculture and Forestry Sciences*, *Beijing* 100097, *China*

ABSTRACT

Hypobaric hypoxia encountered at high altitudes impairs reproductive health and fertility across species. Previous findings have demonstrated that maternal hypoxia exposure disrupts granulosa cell (GC) viability and oocyte maturation in female offspring; however, its transgenerational impact on male reproductive outcomes remains poorly elucidated. In this study, pregnant mice (F0) were subjected to hypoxic conditions, and male progeny across four generations (F1–F4) were evaluated. Results revealed that maternal hypoxia induced mild alterations in sperm DNA methylation in F1 males but caused profound developmental defects in F2 embryos, predominantly affecting males. Following mating of F1 males with control females, a substantial proportion of male F2 fetuses were lost at embryonic day (E) 13.5, attributed to placental malformations. Integrated RNA sequencing and whole-genome bisulfite sequencing of placentas from male fetuses revealed aberrant expression of imprinted genes, including *Gnas*, *Slc38a4*, *Jade1*, and *Kcnq1*, which also exhibited differential methylation in F1 sperm. These findings demonstrate that maternal hypoxia disrupts epigenetic programming in F1 germ cells, impairing placental development and fetal viability in F2 males, thereby leading to an unbalanced sex ratio. Overall, this study elucidates the mechanisms by which environmental hypoxia influences sex ratios and offers critical insights into hypoxia-induced reproductive impairments in mammals.

Keywords: Maternal hypoxia; Sex ratio; Placenta; DNA methylation; Imprinted genes

INTRODUCTION

Globally, over 81 million individuals reside at elevations above 2 500 m a.s.l., with approximately 14.4 million living beyond 3 500 m a.s.l. (Tremblay and Ainslie, 2021). Hypobaric hypoxia, the defining feature of high-altitude environments, imposes considerable physiological stress on unacclimated mammals, adversely affecting cardiovascular health, pulmonary function, and reproductive competence (Mallet et al., 2021; Moore, 2017; Yan, 2014). As a potent environmental determinant of health and disease, hypoxia shapes biological outcomes in both human and animal populations inhabiting high-altitude areas (Julian and Moore, 2019; Simonson et al., 2010). In adult mice, high-altitude-induced hypoxia perturbs endocrine homeostasis by modulating the levels of gonadotropins and steroid hormones via altered metabolic pathways (Marcouiller et al., 2021). In humans, chronic hypoxic exposure leads to a decrease in plasma testosterone concentrations and testicular vasodilation (Alcantara-Zapata et al., 2022) (Fahim et al., 1980). Hypoxia-induced oxidative stress also triggers extensive germ cell apoptosis, culminating in marked declines in sperm counts (Jankovic Velickovic and Stefanovic, 2014). Furthermore, recent studies suggest that paternal hypoxic exposure exerts intergenerational effects, impairing offspring development and spermatogenesis (Li and Yang, 2022), potentially via germline-dependent mechanisms. These findings collectively implicate hypoxia as a disruptor of reproductive integrity with the capacity for heritable transmission of dysfunction.

Received: 08 March 2025; Accepted: 26 May 2025; Online: 27 May 2025

Foundation items: This work was supported by the National Natural Science Foundation of China (32400711, U22A20447), Natural Science Foundation of Qinghai (2025-ZJ-910Q), and “Kunlun Talents” Project from the Qinghai Provincial Government (to Q.E.Y.)

[#]Authors contributed equally to this work

*Corresponding authors, E-mail: hou@cau.edu.cn; yangqien@nwipb.cas.cn

However, it remains unclear whether maternal hypoxia exposure elicits epigenetic modifications that extend across generations to affect the reproductive health and developmental trajectories of non-exposed descendants.

Exposure to high-altitude hypoxic conditions during pregnancy compromises maternal-fetal homeostasis, with long-lasting consequences for offspring viability and reproductive outcomes (Savu et al., 2012). In such environments, maternal physiology is tightly regulated to optimize oxygen delivery to the fetus, although these compensatory responses may be insufficient to prevent developmental disruption. Hypoxia may damage the uterus or placenta and induce epigenetic modifications in fetal tissues, including the liver and vasculature, that perturb normal developmental programs (Soares et al., 2017). Moreover, acute episodes of uteroplacental ischemia-hypoxia can inflict oxidative damage to the fetal brain, with long-term neurological implications (Jiang et al., 2021). Notably, recent research has revealed heightened vulnerability of male fetuses to hypoxic stress during gestation, contributing to sex-biased fetal loss (He et al., 2022) and implicating hypoxia as a driver of sexual dimorphism in developmental outcomes. However, the extent to which maternal hypoxia exposure affects male fertility and developmental capacity in successive generations has not yet been evaluated.

Environmental hypoxia during gestation exerts its developmental effects primarily through the maternal-fetal interface, with the placenta serving as the principal conduit for environmental signal transmission. As a transient, highly specialized organ, the placenta maintains embryonic development during mammalian pregnancy, orchestrating the bidirectional exchange of nutrients, gases, and waste between maternal and fetal circulations, thereby ensuring an appropriate environment for embryonic development (Malassiné et al., 2003) . Its development is uniquely governed by both maternal and paternal genomes, reflecting a coordinated epigenetic program essential for optimal fetal outcomes (Mcgrath and Solter, 1984). Emerging evidence indicates that paternal environmental exposures—including circadian disruption, dietary imbalance, and metabolic stress—can impair placental function and indirectly compromise offspring development (Bhadsavle and Golding, 2022) (Lassi et al., 2021) Such perturbations have been linked to epigenetic remodeling at key imprinted loci, including sex-specific alterations in placental gene expression and methylation profiles of *Peg3*, *Peg9*, and *Peg10* in models of paternal obesity (Mitchell et al., 2017). These findings underscore the importance of paternal epigenetic contributions to placental health and implicate DNA methylation of imprinted genes as a central mechanism mediating intergenerational transmission of environmental effects (Cassidy and Charalambous, 2018; Tycko and Morison, 2002). Several mouse models with targeted disruption of specific imprinted genes have demonstrated that fetal and placental growth may be regulated by such genes (Susiarjo et al., 2013). While previous studies have explored intrauterine hypoxia as a disruptor of placental function, its impact on imprinted gene regulation—particularly at the level of DNA methylation—remains poorly understood.

To replicate natural high-altitude conditions more faithfully, mice were housed under a natural high-altitude, low-oxygen environment (3 300 m a.s.l., 106 mmHg partial oxygen pressure (PaO_2)) rather than in a hypoxic chamber. In this study, the effects of maternal hypoxia exposure from embryonic day (E) 0.5 to 16.5 (F0) were systematically investigated across three generations (F1–F4) to evaluate its transgenerational influence on offspring development and reproductive outcomes. Maternal exposure to environmental hypoxia resulted in altered DNA methylation profiles in sperm from F1 adult males and caused male-biased fetal loss in the F2 generation at E13.5, associated with severe placental defects. Notably, this phenotype was confined to the F2 generation. Integrative transcriptomic and whole-genome bisulfite sequencing (WGBS) analyses of F2 male placentas identified widespread dysregulation of imprinted genes, including *Slc38a4*, *Jade1*, *Kcnq1*, and *Gnas*, which also exhibited differential methylation in F1 sperm following hypoxia exposure. Together, these results provide a mechanistic framework for understanding how maternal hypoxia disrupts intergenerational reproductive outcomes through imprinting-related placental dysfunction, with implications for embryonic development, sex ratio bias, and epigenetic inheritance in mammals.

MATERIALS AND METHODS

Reagents

All reagents used in this study were purchased from Millipore Sigma (USA) unless otherwise stated.

Ethical approval

All experimental procedures involving animals were approved by the Laboratory Animal Care and Use Committee of the Northwest Institute of Plateau Biology, Chinese Academy of Sciences (Approval No. NWIPB2024-1-2).

Animal treatment

Seven-week-old CD-1® mice were purchased from the Beijing Vital River Experimental Animals Centre (Beijing, China) and housed under standard conditions with a 12 h light-dark cycle (from 0800h to 2000h) at the Department of Animal Experiments. A total of 200 female and 100 male mice were included in the study. Control females were derived from dams mated and maintained under normoxic conditions (50 m a.s.l., 150 mmHg PaO_2) at the Central Animal Laboratory of the Institute of Zoology, China Agricultural University. In contrast, hypoxia-exposed female mice were derived from dams mated and maintained under natural hypobaric hypoxia (3 300 m a.s.l., 106 mmHg PaO_2) at the National Field Scientific Observation and Research Station of the Alpine Grassland Ecosystem in Tibetan Autonomous Prefecture of Haibei (Figure 1A). All animals received identical feed and purified drinking water sourced from the same suppliers to ensure environmental consistency.

Mating procedures were performed as previously described (Wang et al., 2018). Pairings occurred between 1630h and 1730h, with vaginal plug checks conducted the following morning between 0830h and 0930h; detection of a plug was designated as embryonic day 0.5 (E 0.5). Hypoxic exposure of pregnant females spanned E0.5 to E16.5, after which the animals were transported to the Central Animal Laboratory of the Institute of Zoology, China Agricultural University, for parturition under normoxic conditions. Previous investigations assessing the impact of environmental transitions on maternal stress responses during pregnancy reported no significant physiological alterations in dams (Zhang et al., 2024a; Zhang et al., 2024b). These findings indicate that brief environmental

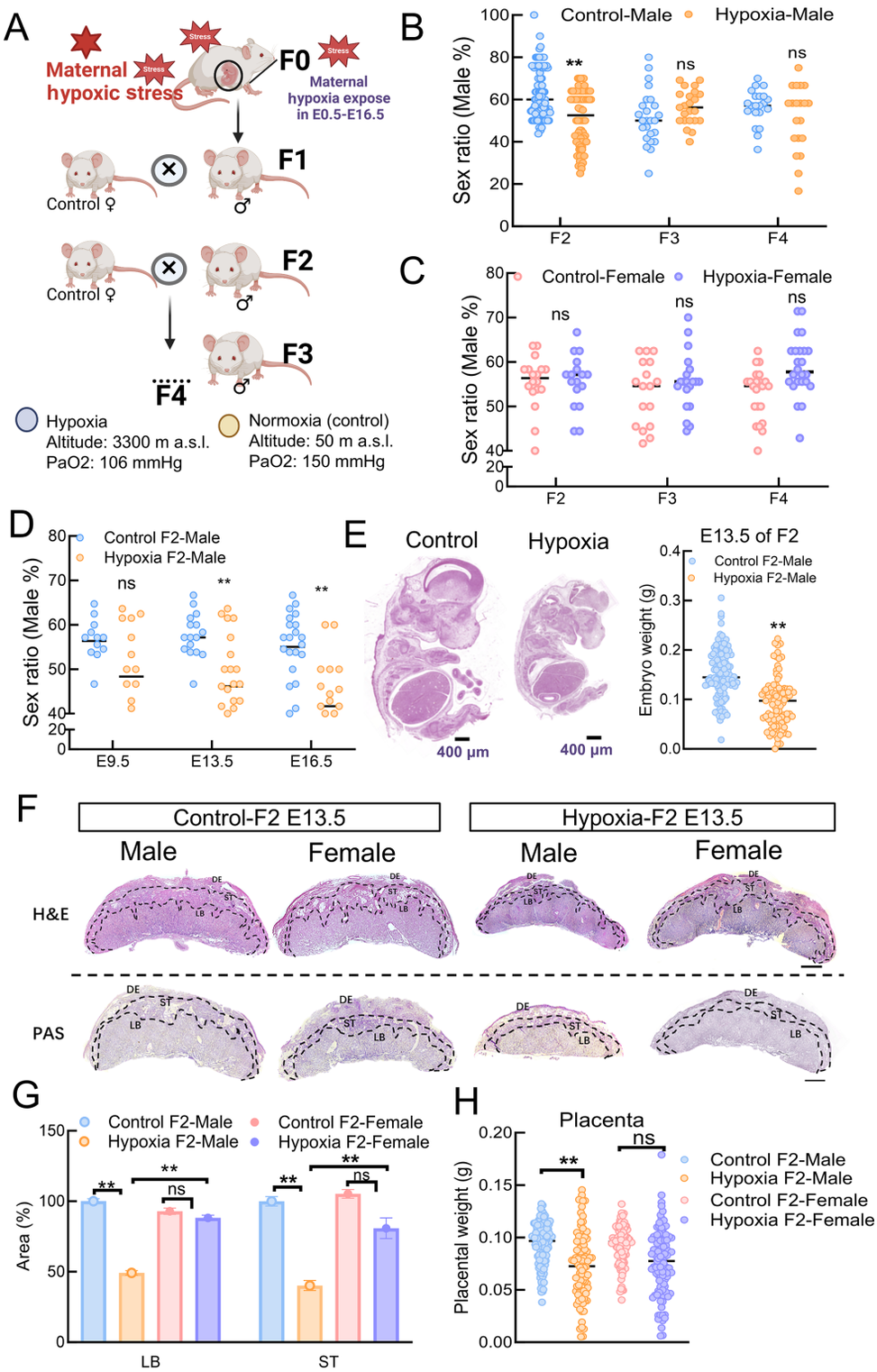

Figure 1 Maternal hypoxia alters fetal sex ratio across generations

A: Schematic of maternal hypoxia exposure in a male mouse model. B: Sex ratio (male%) in control and hypoxia-male groups in F2–F4 generations. C: Sex ratio (male%) in control and hypoxia-exposed females (F2: control *n*=18, hypoxia: *n*=17; F3: control: *n*=18, hypoxia: *n*=20; F4: control: *n*=23, and hypoxia: *n*=24). D: Embryonic sex ratios (male%) at E9.5, E13.5, and E16.5 (E9.5 control-male: *n*=14, hypoxia-male: *n*=16; E13.5 control-male: *n*=18, hypoxia-male: *n*=23; E16.5 control-male: *n*=18, and hypoxia-male: *n*=26). E: Representative H&E-stained images of E13.5 embryos from control and hypoxia-exposed F1 males. Scale bar: 400 μm. Embryo weights at E13.5 (control F1-male: *n*=112 and F1-male: *n*=94). F: Representative H&E- and PAS-stained sections of E13.5 placentas from control and hypoxia groups (F2-male and F2-female). DE, decidua; ST, spongiotrophoblast layer; LB, labyrinth layer. Scale bar: 400 μm. G: Quantification of LB and ST layer areas from placental sections (control F2-male: *n*=6, hypoxia F2-male: *n*=20, control F2-female: *n*=5, and hypoxia F2-female: *n*=16). H: Placental weight at E13.5. Note: placental weight was significantly lower in male embryos (control F2-male: *n*=113, F2-male: *n*=95, control F2-female: *n*=103, and F2-female: *n*=102). Results are presented as mean±SD. All experiments were repeated at least three times. ns: Not significant; *: $P<0.05$; **: $P<0.01$.

changes during transport had negligible effects on maternal physiology.

Experimental housing equipment at both the Haibei Station and China Agricultural University was standardized using apparatus from Suzhou Monkey Emperor Animal Experimental Equipment Technology Co., Ltd. These systems maintained constant temperature, humidity, and photoperiod, with filtered air circulation. Identical batches of purified water (NongFu Spring), sterilized feed, and bedding (Beijing HuaFuKang Biotechnology Co., Ltd.) were used throughout to ensure consistency and reduce confounding variables. Evaluation of blood physiological indices in pregnant mice exposed to short-term hypoxia revealed no significant changes in immune markers, such as white blood cell counts (Supplementary Table S1), indicating minimal maternal immune response to transient hypoxic exposure.

DNA extraction and WGBS

Genomic DNA was extracted from 50 mg of placental tissue using an Axygen DNA Extraction Kit according to the manufacturer's instructions.

WGBS Library construction

Qualified DNA samples were spiked with a defined proportion of unmethylated lambda DNA (negative control) and subsequently fragmented to 200–300 bp. Fragmented DNA underwent bisulfite treatment using an Accel-NGS® Methyl-Seq DNA Library Kit, which converts unmethylated C to U (T after polymerase chain reaction (PCR) amplification), while methylated C remains unchanged. PCR amplification was performed to introduce sequencing adapters, generating the final bisulfite-converted DNA libraries.

WGBS Library quality control

Initial library concentration was assessed using a Qubit 2.0 fluorometer (Thermo Fisher Scientific, USA) and diluted to 1 ng/μL. Fragment size distribution was evaluated using an Agilent 2100 Bioanalyzer (Agilent, China). Libraries meeting quality criteria were subjected to qPCR to quantify effective concentrations, ensuring values exceeded 2 nmol/L prior to sequencing.

An average of 3.32×10^8 sequencing data points were obtained from the WGBS library, including 5 672 differentially methylated regions (DMRs) targeting 3 526 differentially methylated genes (DMGs). In sperm WGBS libraries, sequencing yielded an average of 8.16×10^8 reads with an average alignment rate of 88.84%. In addition, mean global methylation levels in placental tissues were 46.17% in controls and 45.27% in hypoxia-exposed F1 males.

WGBS Computer sequencing

High-throughput sequencing was performed on the Illumina HiSeq (Illumina, USA). Libraries were pooled based on effective concentration and target data volume. Four fluorescently labeled dNTPs were sequentially incorporated into flow cells, and fluorescence signals were captured and converted into sequencing peaks using computer software (FastQC, Bismark, Bowtie2) thus obtaining the sequence information of the fragment to be tested.

Raw image data from the sequencer were processed using the CASAVA pipeline for base calling and converted to FASTQ file format. Adapter trimming and quality filtering were performed to generate clean reads. Methylation mapping was conducted using Bismark, which applies bisulfite-aware alignment via Bowtie2. Both the sequencing reads and reference genome were converted (C-to-T on forward strands and G-to-A on reverse complements) to enable accurate alignment. Bismark then generated genome-wide cytosine methylation profiles by reporting base-resolution comparisons across all read alignments.

RNA sequencing (RNA-seq) sample collection and preparation

Total RNA integrity was assessed using an RNA Nano 6000 Assay Kit on the Agilent Bioanalyzer 2100 system (Agilent Technologies, USA). For each sample, 1 μg of RNA was used as input for library preparation. Briefly, mRNA was purified from total RNA using poly-T oligo-attached magnetic beads, followed by fragmentation with divalent cations in First Strand Synthesis Reaction Buffer (5×) under elevated temperature. The PCR products were purified AMPure XP system (BECKMAN COULTER, USA), and library quality was assessed using the Agilent Bioanalyzer 2100 system. Indexed libraries were clustered on the cBot Cluster Generation System using a Tru-Seq PE Cluster Kit v3-cBot-HS (Illumina, USA) according to the manufacturer's instructions. After cluster generation, paired-end sequencing (150 bp) was performed on the Illumina NovaSeq platform (Illumina, USA).

Quantitative real-time polymerase chain reaction (qPCR)

Total RNA was extracted using the RNeasy MicroRNA Isolation Kit (Qiagen, USA) following the manufacturer's instructions. Samples were treated with DNase I, followed by cDNA synthesis using Transcript Uni All-in-One cDNA Synthesis SuperMix (TransGen Biotech, China). RNA concentrations were measured using a Nanodrop 2000 Spectrophotometer (Biolab, Australia). Reactions were carried out on the ABI 7500 real-time PCR system (Thermo Fisher Scientific, USA) using a Fast 96-well Thermal Cycler (Applied Biosystems, USA). Relative gene expression was calculated using the $2^{-\Delta\Delta CT}$ method. The primers used for amplification are shown in Supplementary Table S2.

Histological and immunofluorescence analyses

Placentas and testes were fixed in 4% paraformaldehyde (PFA) at 4°C, dehydrated stepwise through an ethanol gradient, and embedded in paraffin. Tissue sections (5 μm) were cut using a Leica RM2235 microtome (Leica, Germany). Following deparaffinization and rehydration, the sections were stained with hematoxylin and eosin (H&E). For immunofluorescence, antigen retrieval was performed by boiling the sections in 10 mmol/L sodium citrate buffer (pH 6.0) for 20 min. After cooling to room temperature, the samples were washed in phosphate-buffered saline (PBS) and blocked with 10% donkey serum in PBS for 1 h. The sections were subsequently incubated with primary antibodies diluted in PBS containing 3% bovine serum albumin (BSA) at 4°C overnight. After washing in PBS, the sections were incubated with secondary antibodies for 2 h at room temperature, washed again in PBS, and incubated with 4',6-diamidino-2-phenylindole (DAPI) and mounted on slides for immunofluorescence analysis with a Leica DMR fluorescence microscope (Leica, Germany).

Immunohistochemical analysis

Placentas and testes were fixed in buffered PFA (4%), embedded in paraffin, sectioned to approximately 5 μm, and mounted on glass slides. The tissue sections were then deparaffinized in xylene, rehydrated, and retrieved via microwave heating with citrate antigen retrieval solution

(Beyotime, China) for 20 min. Endogenous peroxidase activity was quenched by incubation with 3% H_2O_2 for 10 min. After blocking in 10% goat serum for 1 h, the sections were stained with different primary antibodies (dilutions are shown in Supplementary Table S3). Corresponding secondary antibodies were conjugated with biotin-labeled antibodies.

Cell proliferation assay (CCK-8)

Granulosa cells (GCs) were seeded at a concentration of 1×10^4 cells per well in 96-well plates and incubated at 37°C for 48 h. Cell viability was assessed using the Cell Counting Kit-8 (CCK-8) (Beyotime, China) according to the manufacturer's instructions. Subsequently, 10 μL of CCK-8 solution was added to the wells and incubated for an additional 2 h. Optical density (OD) values were detected with a microplate reader (TECAN, Switzerland) at 450 nm.

EdU assay

Cell proliferation was evaluated using the EdU Cell Proliferation Kit with Alexa Fluor 594 (Beyotime, China), following the provided guidelines. Cells were harvested and plated at a density of 1×10^5 cells per well in 48-well plates and incubated with 20× EdU labeling reagent at 37°C for 40 min. Fluorescence imaging was performed using an FLUOVIEW FV1000 fluorescence microscope (Olympus, Japan).

Mitochondrial membrane potential *(Δφm)* assay

Mitochondrial membrane potential was measured using a JC-1 Dye Assay Kit (Beyotime, China). Cells were cultured in 48-well plates and incubated with 10 μmol/L JC-1 working solution at 37°C under 5% CO_2 for 20 min. After staining, cells were washed three times with Dulbecco's Phosphate-Buffered Salin (DPBS) to remove excess dye and imaged using a fluorescence microscope (Olympus, Japan). JC-1 aggregates, indicative of high *Δφm*, emitted red fluorescence, whereas JC-1 monomers, indicative of low *Δφm*, emitted green fluorescence. The red-to-green fluorescence ratio was used to quantify *Δφm*.

Adenosine triphosphate (ATP) content assays

Intracellular ATP levels were measured using an Enhanced ATP Assay Kit (Beyotime, China) following the provided guidelines. Cells were seeded in 6-well plates (1×10^6 cells per well). After treatment, cells were harvested and exposed to 20 μmol/L lysis solution in a 0.2 mL RNA-free centrifuge tube, followed by centrifugation at 12 000 ×*g* for 5 min at 4°C, and supernatants were collected. ATP detection reagent was added to white 96-well plates and incubated at room temperature for 3–5 min. Standard ATP solutions (0–40 pmol/μL) and diluted samples were then added to each well. Luminescence was immediately measured using a luminometer Infinite F200 (Tecan, Switzerland). ATP concentrations were calculated based on the standard curves. Total ATP levels were divided by the sample content in each group to quantify the mean ATP concentration (pmol/μL).

Bisulfite sequencing PCR

Bisulfite sequencing was performed as previously described (Cheng et al., 2014), with some modifications. Genomic DNA was subjected to bisulfite treatment according to the manufacturer's instructions (Tiangen, China). Briefly, 500 μL of lysis buffer (1 mmol/L SDS, 10 mmol/L Tris-HCl, 100 mmol/L ethylenediaminetetraacetic acid (EDTA), 280 μg/mL proteinase K) was added to each sample, followed by incubation at 56°C overnight. DNA denaturation was achieved by equilibration in 0.3 mol/L NaOH (500 μL) for 15 min, repeated twice at room temperature. Samples were then treated with 500 μL of freshly prepared bisulfite solution (2.5 mol/L sodium metabisulfite, 125 mmol/L hydroquinone; pH = 5) and incubated at 50°C for 8 h in the dark. Reactions were terminated by incubation with 1 mL of Tris-EDTA (TE) buffer for three consecutive 15 min intervals. This was followed by equilibration in 500 μL of 0.3 mol/L NaOH for two 15 min intervals, sequential washes with TE buffer (2×15 min) and H_2O (2×15 min), and either storage at −20°C or downstream PCR analysis.

The PCR products were subjected to bisulfite conversion using an EZ DNA Methylation Direct Kit (Zymo Research, USA). Nested PCR was performed via methylation-specific DNA polymerase (Tiangen, China). Both first- and second-round amplification were performed under the following thermocycling conditions: 2 min at 95°C, followed by 30 cycles of PCR consisting of 30 s at 94°C, 30 s at annealing temperatures, and 1 min at 72°C. The PCR products were separated by electrophoresis on a 1% agarose gel, and the correct bands were excised and purified using a QIAquick Gel Extraction Kit (Qiagen, Germany). The purified DNA was subsequently cloned and inserted into a pDM18-T vector (TaKaRa, Japan) according to the manufacturer's instructions. Methylation levels were determined by calculating the number of methylated CpGs relative to the total number of CpG sites per clone. Clones with more than 50% CpG methylation were considered hypermethylated.

RNA-seq data analysis

Differential gene expression analysis between control and treated animals (two biological replicates per condition) was performed using the DESeq2 R package (v.1.20.0). DESeq2 employs a generalized linear model based on the negative binomial distribution to estimate differential expression from count-based RNA-seq data. *P*-values were adjusted using the Benjamini-Hochberg approach to control the false discovery rate (FDR). Genes with adjusted $P<0.05$ were defined as differentially expressed.

Gene Ontology (GO) and Kyoto Encyclopedia of Genes and Genomes (KEGG) enrichment analysis

GO enrichment analysis of differentially expressed genes (DEGs) was performed using the clusterProfiler R package (v.4.3.2), which accounts for gene length bias. GO terms with adjusted $P<0.05$ were considered significantly enriched. KEGG pathway analysis was also performed using clusterProfiler to assess the statistical overrepresentation of DEGs in functional pathways. The KEGG database (www.genome.jp/kegg/) provides comprehensive information on high-level biological processes, including cellular and organismal systems, based on large-scale molecular datasets generated by genome sequencing and other high-throughput experimental technologies.

Alternative splicing (AS) analysis

AS events were identified using the rMATS software package (v3.2.5), which enables detection of differential splicing patterns across experimental conditions. AS was analyzed as a regulatory mechanism contributing to transcriptomic complexity.

Protein-protein interaction (PPI) analysis of DEGs

PPI networks among DEGs were analyzed using the Search Tool for the Retrieval of Interacting Genes/Proteins (STRING)

database, which integrates known and predicted interactions from multiple sources to explore functional connectivity.

Statistical analysis

All experiments were independently repeated at least three times. Data are presented as mean±standard deviation (SD), unless otherwise specified. Statistical analyses were performed using SPSS (v.19.0). Statistical comparisons were made using analysis of variance (ANOVA) or Student's *t*-tests. $P<0.05$ was considered statistically significant.

RESULTS

Maternal hypoxia exposure disrupts sex ratio in F2 offspring

To evaluate the impact of environmental hypoxia exposure during fetal development, pregnant F0 mice were exposed to natural high-altitude hypoxia (3 300 m a.s.l., 106 mmHg PaO_2) from E1 to E16.5 and subsequently transferred to a normoxic vivarium at low altitude (50 m a.s.l., 150 mmHg PaO_2). F1 offspring were born and raised under normoxic conditions (Figure 1A). After reaching sexual maturity, F1 males were mated with control females to generate F2 progeny, and this mating scheme was extended to produce F3 and F4 generations. In this model, only the F1 germline experienced indirect hypoxic exposure.

Fertility assessments revealed a slight decrease in male reproductive capacity in F1, but a significant decline in F2 (Figure 1B; Supplementary Figure S1A). Strikingly, the F2 generation exhibited a distorted sex ratio, with a marked reduction in male offspring compared to controls (62.26% females vs. 50.89% in controls; $P<0.001$) (Table 1). This skewing was attributed to selective loss of male fetuses before parturition and was confined to the F2 generation, with no deviations in sex ratio observed in F3 or F4 newborns (Figure 1B). Furthermore, normal sex ratios were restored in progeny produced by F2 or F3 females mated with control males (Figure 1C), suggesting that this unique phenotype was specifically transmitted via the male germline.

To determine the developmental timing of male fetal loss, F2 male embryos were genotyped for *Sry* at E9.5, E13.5, and E16.5 (Supplementary Figure S1B). The proportion of male embryos was significantly reduced at E13.5 and E16.5 (Figure 1D). Measurements of embryonic weight and length at E9.5, E10.5, and E12.5 revealed growth retardation initiating around E12.5 (Supplementary Figure S1C, D). By E13.5, hypoxia-exposed F2 male embryos displayed significantly reduced size and weight compared to controls (Figure 1E), indicating the onset of developmental impairment. In addition, reduced body weights and altered organ-to-body ratios were observed in F2 and F3 mice but were fully normalized in the F4 generation (Supplementary Figure S1E–K), indicating intergenerational effects of fetal hypoxia on offspring growth. Taken together, these findings demonstrate that maternal hypoxia induces male-specific embryonic loss in the F2 generation, with developmental impairment emerging at E13.5 and manifesting in a significantly skewed sex ratio at birth.

Maternal hypoxia disrupts placental morphology and induces spongiotrophoblast (ST) apoptosis in F2 male embryos at E13.5

The placenta serves as a transient yet vital interface mediating nutrient, gas, and waste exchange between the mother and fetus during gestation (Turco et al., 2018). At E13.5, placental cross-sectional area was markedly reduced in F2 male embryos derived from hypoxia-exposed lineages, while F2 females displayed no such change, indicating a male-specific vulnerability in placental development (Figure 1F). Histological analysis using periodic acid-Schiff (PAS) staining revealed pronounced architectural disruptions in F2 male placentas, with the ST and labyrinth-trophoblast (LB) layers reduced by 59.75% and 50.85% respectively, compared with controls (Figure 1G). Placental weight displayed a similar pattern (Figure 1H). To assess the cellular basis of these defects, ST layer cells were immunostained with TPABA and analyzed for proliferation and apoptosis (Supplementary Figure S2A, B). Proliferation, measured by PCNA positivity, was diminished by 34.71%, while apoptosis, assessed via TUNEL staining, increased by 28.31% in ST cells of F2 males (Supplementary Figure S2C). In addition, analysis revealed significant reductions in both essential and non-essential amino acid concentrations in E13.5 hypoxia-exposed F2 male embryos (Supplementary Figure S2D, E), suggesting compromised nutrient transport. In summary, these findings indicate that placental development and function are impaired in F2 male embryos following maternal hypoxia exposure, which is likely responsible for the fetal loss observed in this generation.

Maternal hypoxia dysregulates embryo development-related gene expression in F2 male placentas

To investigate transcriptional alterations associated with placental dysfunction, RNA-seq was performed on E13.5

Table 1 Sample sizes used for statistical analysis of average litter size, offspring sex ratio, and embryonic sex ratio at E9.5, E13.5, and E16.5 in hypoxia-exposed F2 groups

Average litter size in different generations					
Control	21		Hypoxia-F1		19
Control	79		Hypoxia-F2		39
Control	25		Hypoxia-F3		23
Control	21		Hypoxia-F4		20
Sex ratio after birth in different generations					
Control	22		Hypoxia-F1		19
Control	105		Hypoxia-F2		76
Control	25		Hypoxia-F3		23
Control	21		Hypoxia-F4		20
Sex ratio at E9.5, E13.5, and E16.5 in hypoxia-F2 generation					
E9.5	Control	14	Hypoxia-F2	16	
E13.5	Control	18	Hypoxia-F2	23	
E16.5	Control	18	Hypoxia-F2	26	

placentas from control and hypoxia-exposed F2 males. A total of 354 DEGs were identified in hypoxia-exposed placentas, including 147 up-regulated and 207 down-regulated genes (Figure 2A; Supplementary Table S4). Among the down-regulated genes, 133—such as *Bmp5, Brd2, Ccnd3, Dnmt1,* and *Commd1*—were specifically suppressed in F2 males, with no corresponding changes observed in F2 females (Figure 2B, C; Supplementary Table S5). GO enrichment analysis revealed that these DEGs were enriched in embryonic development, mitochondrial function, DNA methylation and demethylation, and apoptotic progress (Figure 2D; Supplementary Figure S3A and Table S6). Gene set enrichment and PPI analyses further revealed suppression of amino acid metabolism and transport pathways were down-regulated in hypoxia-exposed F2 male placentas (Supplementary Figure S3B, C).

To further assess placental impairment at E13.5, trophoblast cells were isolated and cultured *in vitro*. Immunostaining confirmed the identity of $TPABA^+$ trophoblasts (Figure 2E). Cell viability was significantly reduced in hypoxia-exposed F2 males relative to controls (Figure 2F), accompanied by a 16.1% decrease in EdU^+ proliferating cells (Figure 2G; Supplementary Figure S3D). Given the transcriptomic signatures implicating mitochondrial dysfunction, functional assays were conducted. Reactive oxygen species (ROS) levels were elevated in hypoxia-exposed F2 males (Figure 2H), while mitochondrial membrane potential (MMP), ATP content, mitochondrial density, and the expression of mitochondrial function-related genes (*Ndufs1*, *Ndufs3*, *Ndufs4*, and *Sdhb)* were markedly diminished (Supplementary Figure S3E–I). These results suggest that maternal hypoxia compromises mitochondrial integrity and gene networks essential for placental development in F2 male embryos.

Maternal hypoxia alters DNA methylation of imprinted genes in F2 male placentas

To investigate whether DNA methylation contributes to dysregulated gene expression and intergenerational phenotypes (Zhang et al., 2019), WGBS was performed on E13.5 placentas from control and hypoxia-exposed F2 tissues (Figure 3A). No significant differences in global CpG methylation levels were detected between groups (Figure 3B), and methylation across major genomic elements, including promoters, introns, exons, untranslated regions (UTRs), and CpG islands (CGIs), and shores, remained largely unchanged (Figure 3C, D). These findings imply that hypoxia does not induce widespread methylation alterations but rather affects specific genomic loci. Comparative methylome analysis identified 1 722 hypermethylated and 3 950 hypomethylated DMRs in F2 male placentas compared with controls (Figure 3E; Supplementary Table S7). These DMRs were significantly enriched in loci associated with embryonic and placental development, as well as DNA methylation pathways (Figure 3F, G; Supplementary Table S8). Notably, several imprinted genes critical for embryonic and placental development, such as *Kcnq1*, *H13*, *Slc38a4*, *Jade1*, and *Gnas*, were hypermethylated in F2 male placentas (Supplementary Figure S4D, E), implicating dysregulated imprinting as a potential mediator of placental abnormalities following paternal hypoxia exposure.

Integrated WGBS and RNA-seq analyses identify imprinting gene dysregulation in hypoxia-exposed male F2 placentas

DNA methylation is a major epigenetic modification involved in regulating gene expression. To elucidate the relationship between DNA methylation and gene expression alterations in response to fetal hypoxia, WGBS and RNA-seq datasets from E13.5 placentas were integrated (Figure 4A). Analysis of methylation contexts revealed 650, 47, and 129 DMGs in CG, CHG, and CHH contexts, respectively (Figure 4B; Supplementary Figure S5A, B). These genes were significantly enriched in key developmental and signaling pathways, including metabolism, HIF-1 signaling, and PI3K-Akt signaling (Figure 4C; Supplementary Figure S5C, D). As placental development appeared normal in F2 females, a subset of 15 down-regulated genes was identified specifically in F2 males. Validation by qPCR confirmed reduced expression of imprinted genes *Slc38a4*, *Jade1*, *Kcnq1*, *Gnas*, *H13*, and *Grb10*, alongside embryonic development-related genes *St18*, *Lrp1b*, *Epha5*, and *Map2k5* (Figure 4D, E). These findings implicate impaired expression of paternally regulated imprinted genes in the disrupted placental development observed in F2 males.

Maternal hypoxia leads to aberrant DNA methylation of embryonic genes in adult F1 sperm

Epigenetic modifications acquired during development can be stably transmitted across generations through the male germline (Peters, 2014). To evaluate whether in utero hypoxia alters the sperm methylome in adulthood, WGBS was performed on sperm from F1 males exposed to maternal hypoxia (Figure 5A). Following stringent quality control (Supplementary Figure S6A, B), no significant differences in global CpG methylation or methylation across major genomic features were observed compared with controls (Figure 5B, C). However, locus-specific analysis revealed 4 342 DMRs corresponding to 2 612 DMGs, including 1 485 hypermethylated and 2 857 hypomethylated DMRs in F1 males compared with control males (Supplementary Figure S6C). Functional enrichment analysis revealed that these DMRs were highly associated with embryo development and phenotype-modifying pathways (Figure 5D; Supplementary Figure S6D).

Maternal hypoxia leads to aberrant DNA methylation of imprinted genes in adult F1 sperm and F2 male placentas

To assess the intergenerational inheritance of epimutations, WGBS datasets from F1 sperm and F2 male placentas were integrated, identifying 375 shared DMGs, many of which were imprinted (Figure 5E; Supplementary Table S9). Notably, paternally imprinted genes such as *Slc38a4*, *Jade1*, *Kcnq1*, and *Gnas* were significantly down-regulated in methylated DMRs in F1 sperm (Figure 5E). These genes displayed similar methylation alterations in F2 male placentas (Figure 6A, B). Temporal expression analysis confirmed marked down-regulation of these loci at E13.5 in hypoxia-exposed F2 male placentas (Figure 6C). Consistently, protein-level validation demonstrated significantly reduced expression of GNAS, KCNQ1, SLC38A4, and JADE1 in F2 male placental samples (Figure 6D; Supplementary Figure S7A–E). These results suggest hypoxia-induced aberrant DNA methylation in F1 sperm can be stably inherited in offspring and contribute to sexual dimorphism via changes in imprinted gene expression.

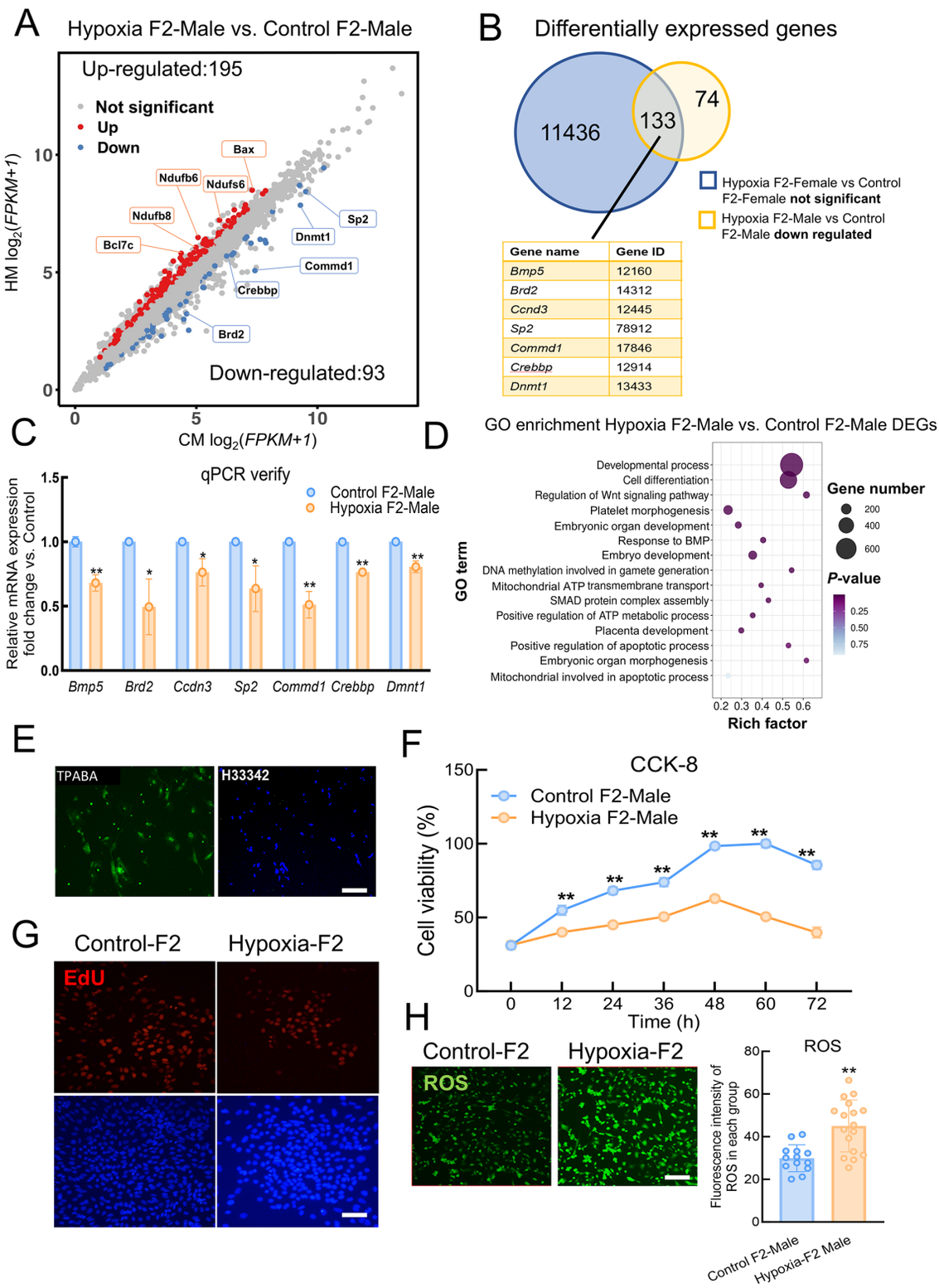

Figure 2 RNA-seq analysis of placental tissues from F2 control and hypoxia-exposed fetuses

A: Volcano plot showing differentially expressed genes (DEGs) in F2 male placentas compared with controls (down-regulated, blue; up-regulated, red); selected highly dysregulated DEGs are annotated. B: Venn diagram showing overlap between genes that were not significantly changed in F2 females versus controls and those down-regulated in F2 males versus controls. C: qPCR validation of selected DEGs (*Bmp5*, *Ccnd3*, *Sp2* and *Dnmt1*), all involved in embryonic development. D: Gene Ontology (GO) enrichment analysis of DEGs in F2 male placentas compared to control F2 males. E: Immunohistochemical staining for TPABA (green) in control and hypoxia-exposed F2 placentas. Scale bar: 50 μm. F: Cell viability of trophoblasts from control and hypoxia-exposed F2 placentas assessed after 12, 24, 36, 48, 60, and 72 h of *in vitro* culture using the CCK-8 assay. G: Representative images showing EdU-labeled cells (red) from control and F2 male placentas. Scale bar: 20 μm. H: Representative fluorescence images of intracellular reactive oxygen species (ROS) levels using 2′7′-dichlorodihydrofluorescein (DCF) staining in control and F2 male placental tissues. Scale bar: 20 μm. Results are presented as mean±SD. ns: Not significant; *: $P<0.05$; **: $P<0.01$.

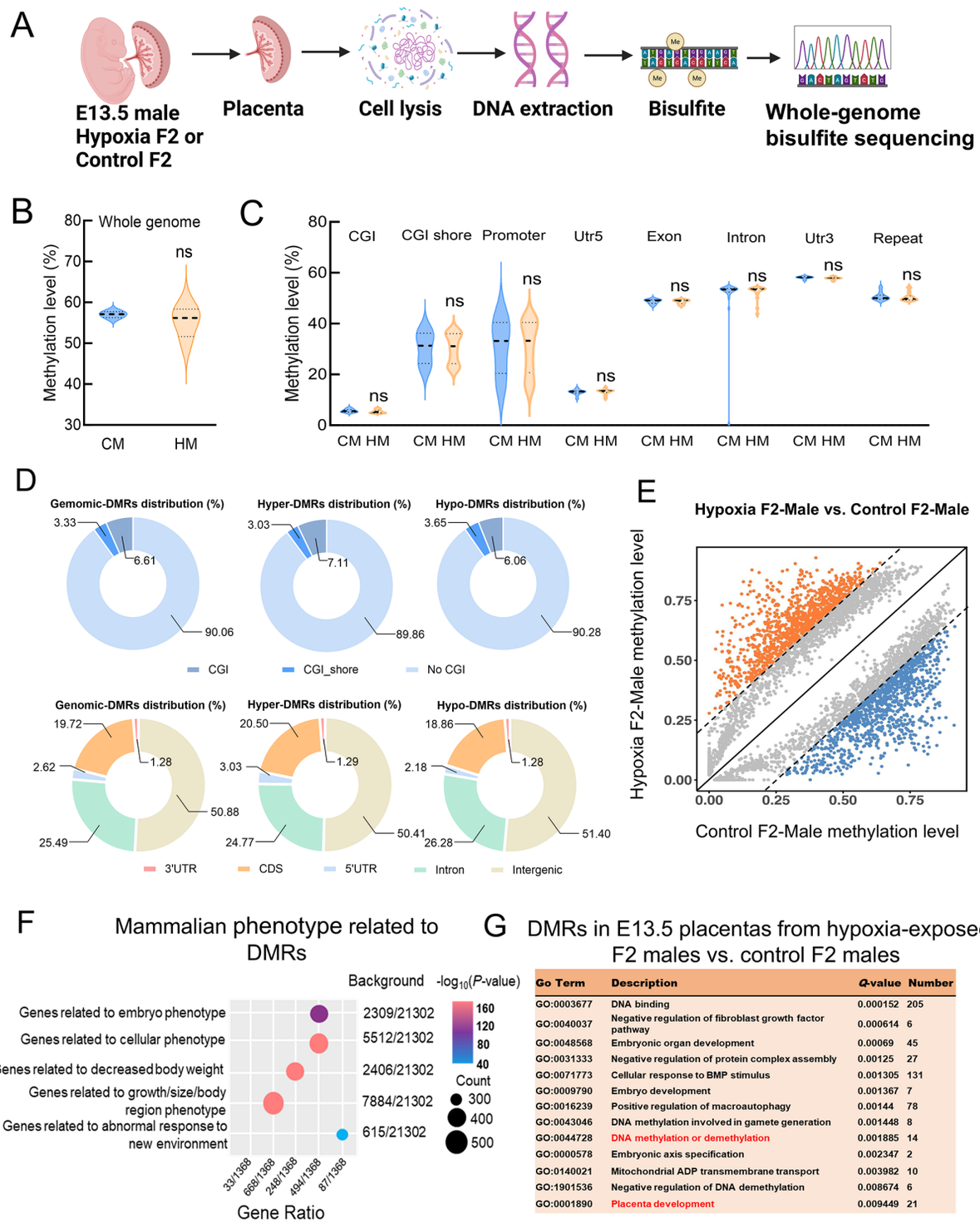

Go Term	Description	Q-value	Number
GO:0003677	DNA binding	0.000152	205
GO:0040037	Negative regulation of fibroblast growth factor pathway	0.000614	6
GO:0048568	Embryonic organ development	0.00069	45
GO:0031333	Negative regulation of protein complex assembly	0.00125	27
GO:0071773	Cellular response to BMP stimulus	0.001305	131
GO:0009790	Embryo development	0.001367	7
GO:0016239	Positive regulation of macroautophagy	0.00144	78
GO:0043046	DNA methylation involved in gamete generation	0.001448	8
GO:0044728	DNA methylation or demethylation	0.001885	14
GO:0000578	Embryonic axis specification	0.002347	2
GO:0140021	Mitochondrial ADP transmembrane transport	0.003982	10
GO:1901536	Negative regulation of DNA demethylation	0.008674	6
GO:0001890	Placenta development	0.009449	21

Figure 3 Whole-genome bisulfite sequencing (WGBS) of placental tissues from control and hypoxia-exposed F2 fetuses

A: Schematic overview of WGBS performed on F2 placental tissues. B: Average genome-wide DNA methylation levels in E13.5 placentas from hypoxia-exposed F2 males (HMs) and control F2 males (CMs). C: Violin plots showing methylation levels across genomic features, including promoters, CGIs, CGI shores, exons, introns, 3'UTRs, and 5'UTRs. D: Distribution of differentially methylated regions (DMRs) across CpG islands (CGIs) and CGI shores (top) and coding versus noncoding regions (bottom). E: Volcano plot depicting hypermethylated and hypomethylated DMRs in control versus F2 male placentas. F: Number of DEGs associated with mouse phenotypes and differential alternative splicing (AS) events in control versus F2-male placentas. G: GO-based functional enrichment analysis of genes associated with DMRs in control and hypoxia-exposed F2 male placentas. Results are presented as mean±SD. ns: Not significant; *: P<0.05; **: P<0.01.

DISCUSSION

This study investigated the effects of maternal hypoxic stress on male offspring development and explored the underlying mechanism across four generations (F1–F4) following *in utero* hypoxia exposure. A striking phenotype emerged in the F2 generation, in which maternal hypoxia selectively induced fetal loss of male progeny, resulting in a skewed sex ratio. Focusing on placental abnormalities in F2 males, integrated

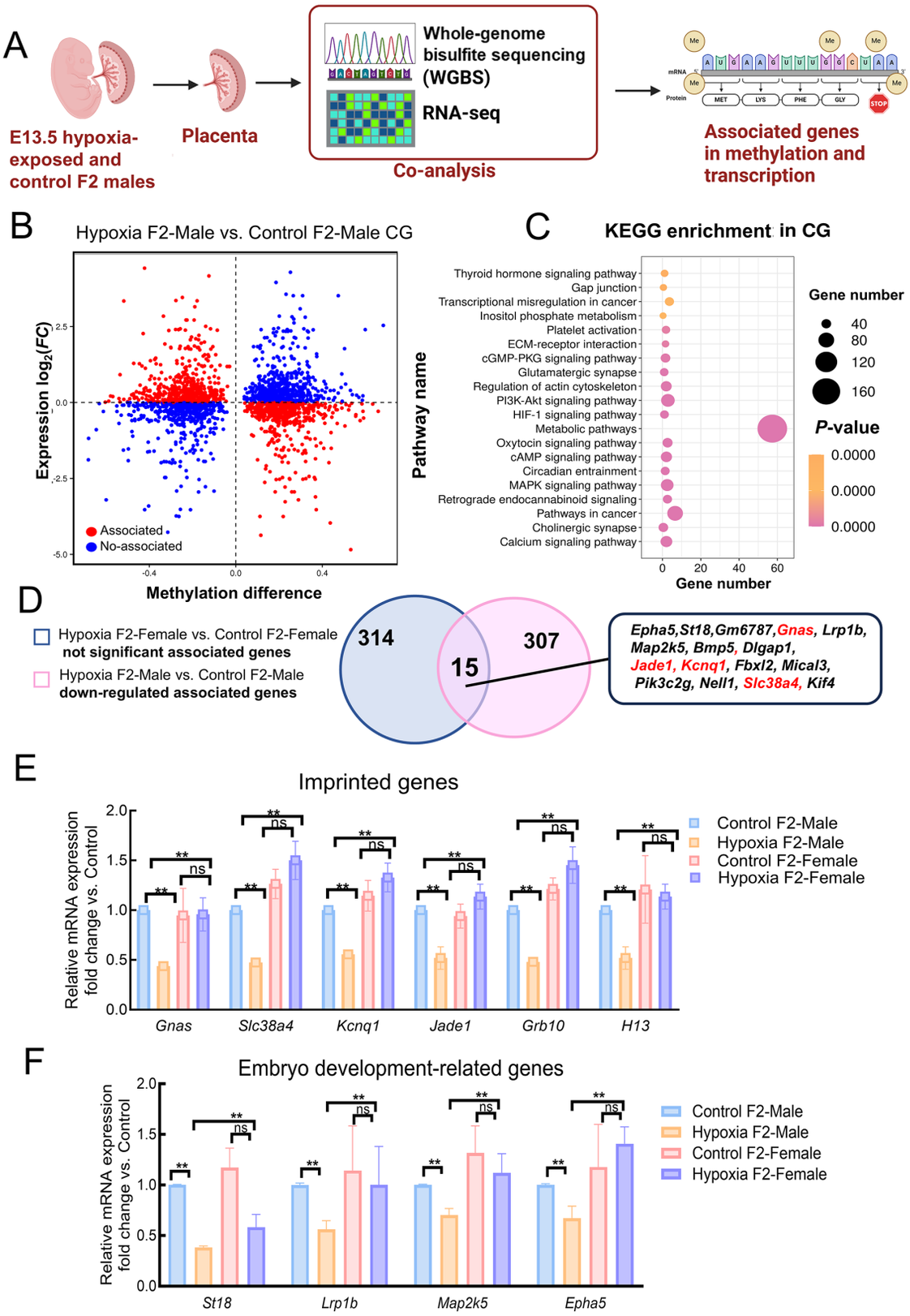

Figure 4 Integrated WGBS and RNA-seq analysis reveals aberrant DNA methylation in placental and embryonic development-related genes in E13.5 placentas

A: Schematic illustration of integrated WGBS and RNA-seq analysis in F2 placentas. B: Volcano plot showing DEGs associated with CpG (CG) regions in hypoxia-exposed F2 male placentas compared with controls (down-regulated, blue; up-regulated, red). C: KEGG pathway enrichment analysis of CG-associated genes in hypoxic versus control F2 male placentas. D: Venn diagram showing overlap between down-regulated genes in F2 males versus controls and F2 female versus controls. E: qPCR validation of embryonic development-related genes, including *Bmp5*, *Slc38a4*, *Jade1*, *Grb10*, *H13* and *Gnas*. F: qPCR validation of embryonic development-related genes, including *St18* and *Epha5*. Results are presented as mean ± SD. qPCR experiments were repeated at least three times. ns: Not significant; *: $P<0.05$; **: $P<0.01$.

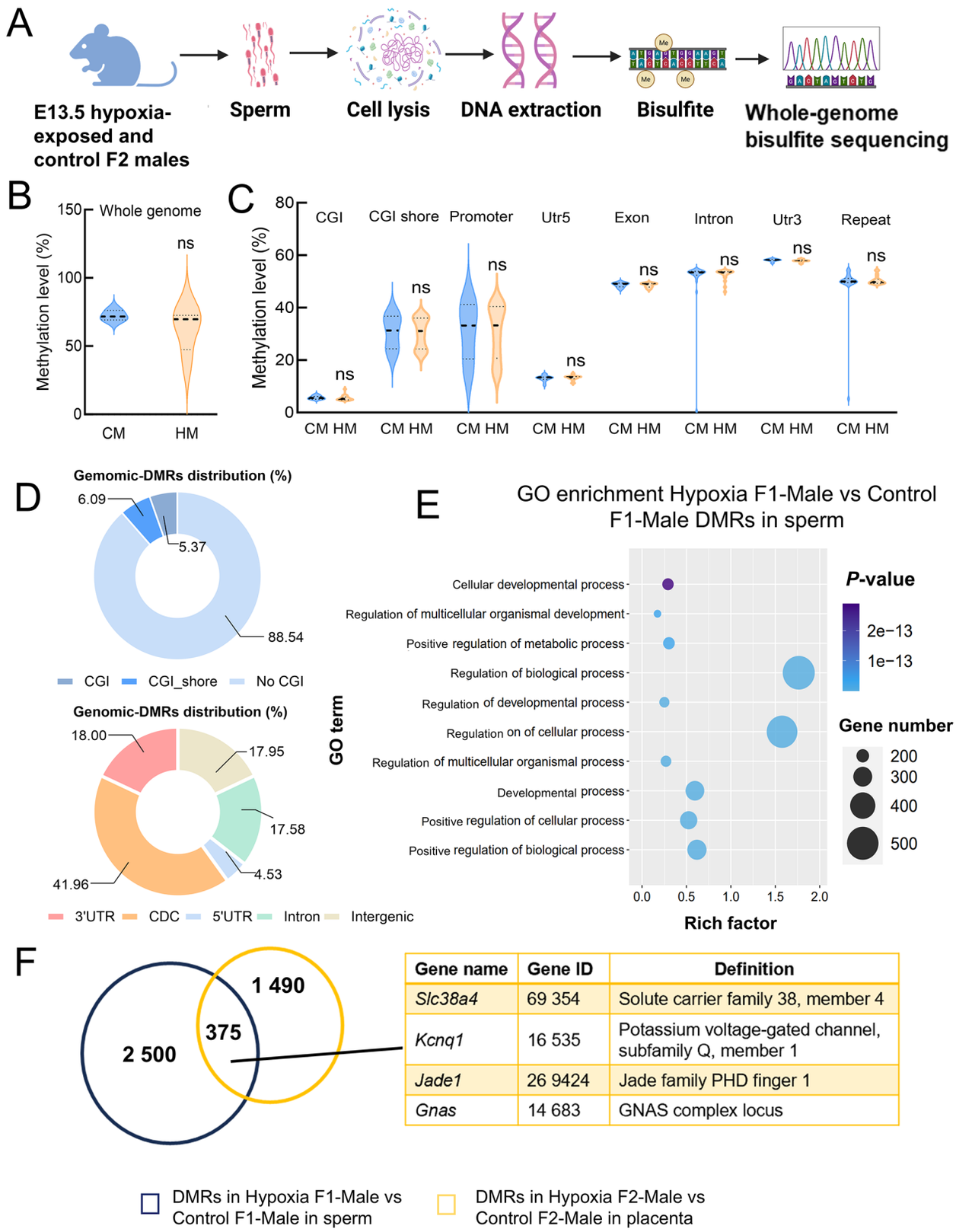

Gene name	Gene ID	Definition
Slc38a4	69 354	Solute carrier family 38, member 4
Kcnq1	16 535	Potassium voltage-gated channel, subfamily Q, member 1
Jade1	26 9424	Jade family PHD finger 1
Gnas	14 683	GNAS complex locus

Figure 5 Combined WGBS analysis of hypoxia-exposed F1 sperm and F2 E13.5 placentas reveals aberrant DNA methylation of imprinted genes

A: Schematic overview of WGBS performed on F1 sperm. B: Average genome-wide DNA methylation levels in sperm from control (CM) and hypoxia-exposed (HM) F1 males. C: Violin plots showing methylation levels across genomic features, including promoters, CGIs, CGI shores, exons, introns, 3'UTRs, and 5'UTRs. D: Relative proportion of DMRs located within CpG islands (CGIs) and CGI shores in control and hypoxia-exposed F1 sperm. E: GO enrichment functional analyses of parental genes associated with DMRs in control-F0 male vs. hypoxia-F1 male sperm. F: Venn diagram showing overlap of hypermethylated paternally imprinted genes between hypoxia-exposed F1 sperm and hypoxic F2 male placentas.

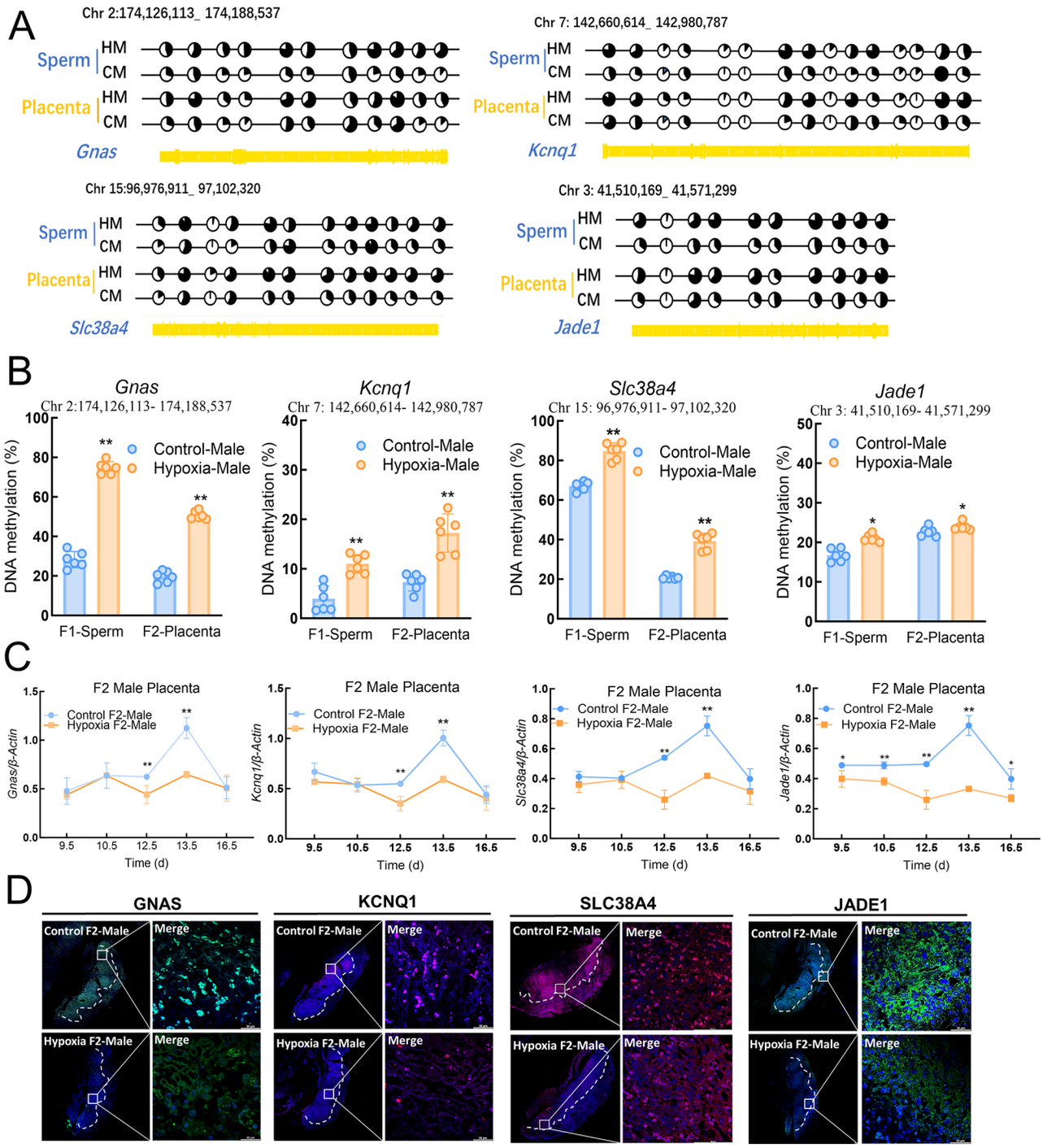

Figure 6 Aberrant DNA methylation of parentally imprinted genes in hypoxia-exposed F1 sperm and E13.5 placentas from hypoxic F2 males

A: Methylation profiles of imprinted genes *Gnas*, *Kcnq1*, *Slc38a4*, and *Jade1* at specific loci in F1 sperm and F2 placentas, with black circles indicating proportion of methylated CpG sites. B: Pyrosequencing of DNA methylation at selected loci within *Gnas*, *Jade1*, *Kcnq1*, and *Slc38a4* in F1 sperm and F2 placentas. C: Gene expression profiles of *Gnas*, *Jade1*, *Kcnq1*, and *Slc38a4* in F2 placentas across different embryonic developmental stages. D: Immunofluorescence staining of placental sections at different embryonic stages showing protein expression of GNAS, KCNQ1, SLC38A4, and JADE1. Nuclei were counterstained with Hoechst 33342 (blue), and relative fluorescence intensities were quantified. Scale bar: 50 μm. Results are presented as mean±SD. Experiments were repeated at least three times. ns: Not significant; *: P<0.05; **: P<0.01.

multiomics analyses identified several key genes, such as *Slc38a4*, *Gnas*, *Jade1*, and *Kcnq1*, with altered expression in hypoxia-exposed F2 male embryos. Methylation analysis revealed that multiple paternally imprinted genes were epigenetically modified in F1 male sperm following maternal hypoxia and that these locus-specific alterations were transmitted to F2 placental tissues (Figure 7). These findings uncover a previously unrecognized role of maternal hypoxia in driving epigenetic reprogramming in F1 sperm, with long-lasting consequences for offspring development.

Hypoxia is a defining feature of high-altitude environments and exerts deleterious effects on both human and animal

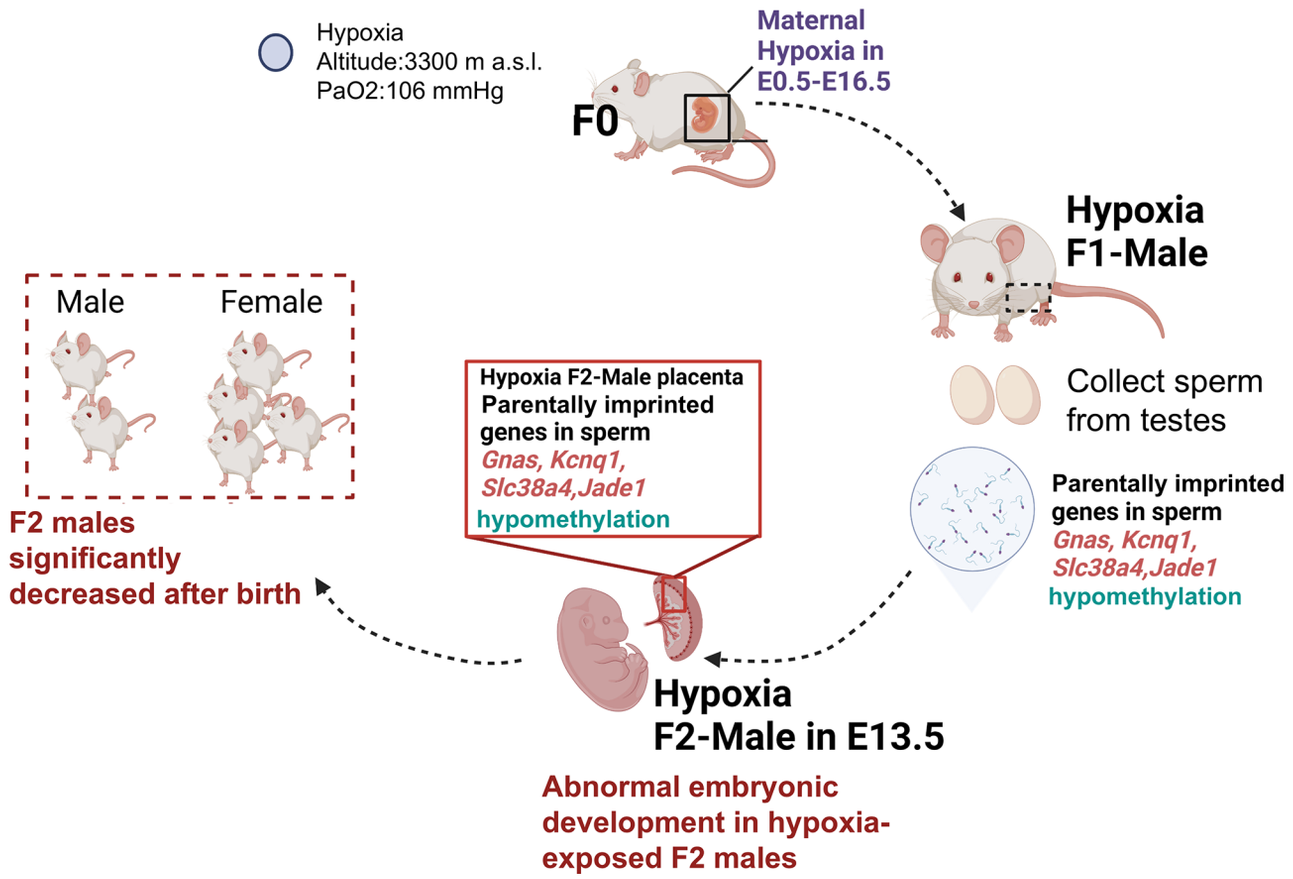

Figure 7 Maternal hypoxia exposure induces aberrant imprinted gene methylation in adult sperm and intergenerational placental impairment in male offspring

A maternal hypoxia exposure model was established to investigate mechanisms underlying developmental impairments in subsequent generations. Results indicated that DNA methylation abnormalities in hypoxia-exposed F1 male sperm were transmitted to offspring, contributing to sex-specific placental defects through dysregulation of imprinted gene expression.

physiology (Julian and Moore, 2019; Mallet et al., 2021; Simonson et al., 2010). While acute and chronic hypoxia have well-established effects on male reproductive function (Li and Yang, 2022; Li et al., 2021; Oyedokun et al., 2023), the intergenerational consequences of developmental hypoxia remain poorly understood in mammals. The timing of exposure during development is critical, with gestational hypoxia known to impair placental structure and induce cardiopulmonary dysfunction in offspring. Previous research has shown that female F1 progeny exhibit a significant reduction in litter sizes and premature reproductive senescence following exposure to hypoxic conditions (Zhang et al., 2024a). In males, hypoxic exposure has been shown to reduce sperm motility, impair pregnancy outcomes, and induce seminiferous tubule damage with increased apoptosis in spermatogenic cells, although these effects are reversible with subsequent normoxic recovery (Li and Yang, 2022; Tao et al., 2022; Verratti et al., 2008). In contrast, hypoxia during fetal development has been linked to persistent metabolic abnormalities in adulthood (Zhang, 2005). Research has also revealed that hypoxia perturbs the entire ovarian endocrine axis, resulting in abnormal estrogen levels, increased GC apoptosis, and enhanced autophagy (Zhang et al., 2024a). These findings collectively underscore the substantial impact of F1 females on the phenotype of F2 progeny. In contrast, F1 males exposed to fetal hypoxia did not exhibit overt reproductive deficits. Although reduced birth weight was observed in F1 females, no sex ratio imbalance was detected at birth, highlighting a distinctive feature of this model. The current study demonstrated that paternal exposure to hypoxia *in utero* resulted in a significant shift in offspring sex ratio in the F2 generation, as revealed through rigorous statistical analysis.

Paternal hypoxia exposure disrupted the sex ratio by inducing male-specific placental defects, with significant loss of male embryos sired by F2 males around E13.5, despite normal sex ratios at E9.5, suggesting no bias during preimplantation or early embryonic development. Placental dysfunction affects embryonic growth and can profoundly influence postnatal outcomes (Deshpande et al., 2023). When placentation is complete, three distinct layers—the decidua, ST, and LB layers—are fully established (Hemberger et al., 2020). Histological analysis revealed reduced placental weight and severe structural damage to the ST and LB layers in F2 male placentas. As deep trophoblast invasion into maternal uterine tissue is essential for proper placental formation (Zhao et al., 2021b), such damage likely impairs developmental support. Consistent with the observation that placentas were morphologically normal in females, no significant changes in global gene expression were detected between control and F2 female placental tissues. Transcriptomic analysis of male placentas revealed altered expression of genes associated with trophoblast differentiation and mitochondrial function regulation following paternal hypoxia exposure, including down-regulation of *Bmp5* and *Brd2*, which are essential for lineage specification and cell proliferation (Zhao et al., 2021b).

Consistently, *in vitro* analysis of ST cells demonstrated decreased JC-1, ATP, and mitochondrial function gene expression. Mitochondrial dysfunction may induce cytochrome c release and electron transport chain leakage, promoting ROS accumulation and oxidative stress. Furthermore, co-analysis of DEGs revealed significant enrichment in amino acid synthesis and metabolic pathways, suggesting that impaired placental energy metabolism contributes to abnormal embryonic development in F2 males.

Epigenetic mechanisms play critical roles in both transgenerational and intergenerational inheritance of environmentally or endogenously induced phenotypic alterations in animals (Wei et al., 2014). Environmental perturbations experienced by the paternal lineage can influence embryonic development through epigenetic modifications or metabolic signals that regulate placental imprinted gene expression (Dietz et al., 2011; Lassi et al., 2021). Genomic imprinting is highly active in extraembryonic tissues such as the placenta and yolk sac (Lassi et al., 2021), and balanced maternal and paternal imprinted gene expression is essential for proper placental function and pregnancy maintenance (Kappil et al., 2015; Lambertini, 2014). In the present study, integrated analyses of genome-wide DNA methylation and transcriptome data from E13.5 placentas revealed that paternal hypoxia exposure during fetal development disrupted both methylation and expression of the paternally imprinted genes *Gnas*, *Jade1*, *Kcnq1*, and *Slc38a4*. These genes are functionally implicated in embryonic and placental development in both humans and mice. For example, G(s)alpha and the alternative G(s)alpha isoform XL-alpha(s), which is expressed from the paternal GNAS allele, exert opposite effects on energy metabolism in mice (Weinstein et al., 2004). The Kcnq1 imprinted domain on distal mouse chromosome 7 contains one paternally expressed gene (Lewis et al., 2006) and two DMRs: a germline DMR acting as the imprinting center (IC2) within the Kcnq1ot1 promoter and a secondary DMR upstream of Cdkn1c, a cell cycle regulator established post-implantation (Bhogal et al., 2004). Jade1 is expressed across multiple embryonic structures, including the pre- and early streak epiblast, primitive streak and node, and, caudal neural hinge, where it regulates differentiation and migration required for anterior-posterior axis elongation (Tzouanacou et al., 2003); (Wilson and Beddington, 1996). Slc38a4 is expressed in chorionic trophoblast cells to promote proliferation during early placental development (Matoba et al., 2019), with its deficiency leading to preterm intrauterine growth restriction (IUGR) pregnancies (Kadife et al., 2022). Collectively, these findings indicate that hypoxia-induced aberrant DNA methylation in F1 sperm is heritable and contributes to sexually dimorphic phenotypes via dysregulated imprinted gene expression.

DNA methylation in the male germline is established during fetal development. Altered methylation patterns of *Gnas*, *Kcnq1*, *Jade1*, and *Slc38a4* were confirmed in F1 sperm. In mice, primordial germ cells (PGCs) migrate to the genital ridge around E10.5–11.5, with gonadal development completing by E13.5, coinciding with a second wave of epigenetic reprogramming (Guo et al., 2015; Hill et al., 2018). Environmental stressors experienced during this pivotal window can disrupt epigenetic programming in PGCs (Heijmans et al., 2008; Ross and Canovas, 2016), potentially altering the epigenetic status of developing gametes. In particular, DNA methylation changes in imprinted genes may indirectly impair embryogenesis by altering placental development. However, with the initiation of epigenetic reprogramming and global demethylation during embryonic development of progeny, some parental imprinting is erased, which may explain the gradual phenotypic recovery observed in F3 and F4 male embryos.

These findings suggest that aberrant DNA methylation of imprinted genes contributes to abnormal embryonic development in male descendants of hypoxia-exposed animals. Such alterations are likely induced by fetal hypoxia and may influence the development of subsequent generations. Nevertheless, the mechanisms by which hypoxia reshapes the methylation landscape of imprinted genes remain unclear. Resolving the basis of imprinting dysregulation is essential for understanding epigenetic responses associated with hypoxic stress. Hypoxia has been shown to restrict embryonic growth and, under severe conditions, result in pregnancy loss (Zhao et al., 2021a). It also disrupts placental and embryonic angiogenesis by affecting VEGF-VEGFR signaling (Ferrara et al., 2003). Low oxygen levels and embryonic angiogenesis can activate HIF-1α, shifting metabolism from oxidative phosphorylation to anaerobic glycolysis (Burton et al., 2017). This metabolic switch may impair epigenetic programming by limiting the production of key metabolites (Reik et al., 2001; Zhao et al., 2021b). It is plausible that maternal hypoxia-induced metabolic changes affect fetal development, thereby initiating intergenerational effects. We propose that epigenetic reprogramming in PGCs during F1 embryogenesis is perturbed by these metabolic shifts, resulting in persistent methylation defects in sperm. In ongoing studies, multi-omics profiling—including metabolomics, epigenomics, and single-cell transcriptomics—is being applied to F1 PGCs to further characterize the impact of in utero hypoxia. The potential role of hypoxia-induced metabolic reprogramming in disrupting germline epigenetic fidelity warrants further investigation.

CONCLUSION

This study established a maternal hypoxia exposure model and elucidated the mechanisms underlying developmental defects in subsequent generations. The findings indicate that hypoxia-induced alterations in DNA methylation in F1 male sperm are heritable and contribute to sex-specific phenotypes in offspring by disrupting the expression of imprinted genes.

DATA AVAILABILITY

All datasets were deposited in the Science Data Bank (DOI: 10.57760/sciencedb.25082), Genome Sequence Archive (GSA, accession No. CRA025649), and National Center for Biotechnology Information (NCBI BioProjectID PRJNA1224843) databases.

SUPPLEMENTARY DATA

Supplementary data to this article can be found online.

COMPETING INTERESTS

The authors declare that they have no competing interests.

AUTHORS' CONTRIBUTIONS

Q.E.Y. contributed to research design. L.Y.Z. contributed to animal research, data analyses, and drafting of the article. G.X.J. participated in the animal experiments. H.P.T., K.X.L., and Y.W.L. participated in animal research and article review. Q.E.Y. and Y.P.H. provided advice on study design, division of labor, and drafting and revision of the paper. All authors read and approved the final version of the manuscript.

REFERENCES

Alcantara-Zapata DE, Llanos AJ, Nazzal C. 2022. High altitude exposure affects male reproductive parameters: could it also affect the prostate?. *Biology of Reproduction*, **106**(3): 385–396.

Bhadsavle SS, Golding MC. 2022. Paternal epigenetic influences on placental health and their impacts on offspring development and disease. *Frontiers in Genetics*, **13**: 1068408.

Bhogal B, Arnaudo A, Dymkowski A, et al. 2004. Methylation at mouse *Cdkn1c* is acquired during postimplantation development and functions to maintain imprinted expression. *Genomics*, **84**(6): 961–970.

Burton GJ, Jauniaux E, Murray AJ. 2017. Oxygen and placental development; parallels and differences with tumour biology. *Placenta*, **56**: 14–18.

Cassidy FC, Charalambous M. 2018. Genomic imprinting, growth and maternal-fetal interactions. *The Journal of Experimental Biology*, **221**(Pt Suppl 1). DOI: 10.1242/jeb.164517

Cheng KR, Fu XW, Zhang RN, et al. 2014. Effect of oocyte vitrification on deoxyribonucleic acid methylation of *H19, Peg3*, and *Snrpn* differentially methylated regions in mouse blastocysts. *Fertility and Sterility*, **102**(4): 1183–1190.

Deshpande SSS, Bera P, Khambata K, et al. 2023. Paternal obesity induces epigenetic aberrations and gene expression changes in placenta and fetus. *Molecular Reproduction and Development*, **90**(2): 109–126.

Dietz DM, Laplant Q, Watts EL, et al. 2011. Paternal transmission of stress-induced pathologies. *Biological Psychiatry*, **70**(5): 408–414.

Fahim MS, Messiha FS, Girgis SM. 1980. Effect of acute and chronic simulated high altitude on male reproduction and testosterone level. *Archives of Andrology*, **4**(3): 217–219.

Ferrara N, Gerber HP, Lecouter J. 2003. The biology of VEGF and its receptors. *Nature Medicine*, **9**(6): 669–676.

Guo F, Yan LY, Guo HS, et al. 2015. The transcriptome and DNA methylome landscapes of human primordial germ cells. *Cell*, **161**(6): 1437–1452.

He YX, Li J, Yue T, et al. 2022. Seasonality and sex-biased fluctuation of birth weight in Tibetan populations. *Phenomics*, **2**(1): 64–71.

Heijmans BT, Tobi EW, Stein AD, et al. 2008. Persistent epigenetic differences associated with prenatal exposure to famine in humans. *Proceedings of the National Academy of Sciences of the United States of America*, **105**(44): 17046–17049.

Hemberger M, Hanna CW, Dean W. 2020. Mechanisms of early placental development in mouse and humans. *Nature Reviews. Genetics*, **21**(1): 27–43.

Hill PWS, Leitch HG, Requena CE, et al. 2018. Epigenetic reprogramming enables the transition from primordial germ cell to gonocyte. *Nature*, **555**(7696): 392–396.

Jankovic Velickovic L, Stefanovic V. 2014. Hypoxia and spermatogenesis. *International Urology and Nephrology*, **46**(5): 887–894.

Jiang J, Giri T, Raghuraman N, et al. 2021. Impact of intrauterine fetal resuscitation with oxygen on oxidative stress in the developing rat brain. *Scientific Reports*, **11**(1): 9798.

Julian CG, Moore LG. 2019. Human genetic adaptation to high altitude: evidence from the Andes. *Genes (Basel)*, **10**(2). DOI: 10.3390/genes10020150

Kadife E, Harper A, De Alwis N, et al. 2022. *SLC38A4* amino acid transporter expression is significantly lower in early preterm intrauterine growth restriction complicated placentas. *International Journal of Molecular Sciences*, **24**(1). DOI: 10.3390/ijms24010403

Kappil M, Lambertini L, Chen J. 2015. Environmental influences on genomic imprinting. *Current Environmental Health Reports*, **2**(2): 155–162.

Lambertini L. 2014. Genomic imprinting: sensing the environment and driving the fetal growth. *Current Opinion in Pediatrics*, **26**(2): 237–242.

Lassi M, Tomar A, Comas-Armangué G, et al. 2021. Disruption of paternal circadian rhythm affects metabolic health in male offspring via nongerm cell factors. *Science Advances*, **7**(22). DOI: 10.1126/sciadv.abg6424

Lewis A, Green K, Dawson C, et al. 2006. Epigenetic dynamics of the *Kcnq1* imprinted domain in the early embryo. *Development*, **133**(21): 4203–4210.

Li S, Yang QE. 2022. Hypobaric hypoxia exposure alters transcriptome in mouse testis and impairs spermatogenesis in offspring. *Gene*, **823**: 146390.

Li ZB, Wang SM, Gong CL, et al. 2021. Effects of environmental and pathological hypoxia on male fertility. *Frontiers in Cell and Developmental Biology*, **9**: 725933.

Malassiné A, Frendo JL, Evain-Brion D. 2003. A comparison of placental development and endocrine functions between the human and mouse model. *Human Reproduction Update*, **9**(6): 531–539.

Mallet RT, Burtscher J, Richalet JP, et al. 2021. Impact of high altitude on cardiovascular health: current perspectives. *Vascular Health and Risk Management*, **17**: 317–335.

Marcouiller F, Jochmans-Lemoine A, Ganouna-Cohen G, et al. 2021. Metabolic responses to intermittent hypoxia are regulated by sex and estradiol in mice. *American Journal of Physiology. Endocrinology and Metabolism*, **320**(2): E316–E325.

Matoba S, Nakamuta S, Miura K, et al. 2019. Paternal knockout of *Slc38a4/SNAT4* causes placental hypoplasia associated with intrauterine growth restriction in mice. *Proceedings of the National Academy of Sciences of the United States of America*, **116**(42): 21047–21053.

McGrath J, Solter D. 1984. Completion of mouse embryogenesis requires both the maternal and paternal genomes. *Cell*, **37**(1): 179–183.

Mitchell M, Strick R, Strissel PL, et al. 2017. Gene expression and epigenetic aberrations in F1-placentas fathered by obese males. *Molecular Reproduction and Development*, **84**(4): 316–328.

Moore LG. 2017. Measuring high-altitude adaptation. *Journal of Applied Physiology*, **123**(5): 1371–1385.

Oyedokun PA, Akhigbe RE, Ajayi LO, et al. 2023. Impact of hypoxia on male reproductive functions. *Molecular and Cellular Biochemistry*, **478**(4): 875–885.

Peters J. 2014. The role of genomic imprinting in biology and disease: an expanding view. *Nature Reviews. Genetics*, **15**(8): 517–530.

Reik W, Dean W, Walter J. 2001. Epigenetic reprogramming in mammalian development. *Science*, **293**(5532): 1089–1093.

Ross PJ, Canovas S. 2016. Mechanisms of epigenetic remodelling during preimplantation development. *Reproduction, Fertility, and Development*, **28**(1–2): 25–40.

Savu O, Jurcuţ R, Giuşcă S, et al. 2012. Morphological and functional adaptation of the maternal heart during pregnancy. *Circulation. Cardiovascular Imaging*, **5**(3): 289–297.

Simonson TS, Yang Y, Huff CD, et al. 2010. Genetic evidence for high-altitude adaptation in Tibet. *Science*, **329**(5987): 72–75.

Soares MJ, Iqbal K, Kozai K. 2017. Hypoxia and placental development. *Birth Defects Research*, **109**(17): 1309–1329.

Susiarjo M, Sasson I, Mesaros C, et al. 2013. Bisphenol a exposure disrupts genomic imprinting in the mouse. *PLoS Genetics*, **9**(4): e1003401.

Tao HP, Jia GX, Zhang XN, et al. 2022. Paternal hypoxia exposure impairs fertilization process and preimplantation embryo development. *Zygote*, **30**(1): 48–56.

Tremblay JC, Ainslie PN. 2021. Global and country-level estimates of human population at high altitude. *Proceedings of the National Academy of Sciences of the United States of America*, **118**(18). DOI: 10.1073/pnas.2102463118

Turco MY, Gardner L, Kay RG, et al. 2018. Trophoblast organoids as a model for maternal-fetal interactions during human placentation. *Nature*, **564**(7735): 263–267.

Tycko B, Morison IM. 2002. Physiological functions of imprinted genes. *Journal of Cellular Physiology*, **192**(3): 245–258.

Tzouanacou E, Tweedie S, Wilson V. 2003. Identification of *Jade1*, a gene encoding a PHD zinc finger protein, in a gene trap mutagenesis screen for genes involved in anteroposterior axis development. *Molecular and Cellular Biology*, **23**(23): 8553–8552.

Verratti V, Berardinelli F, Di Giulio C, et al. 2008. Evidence that chronic hypoxia causes reversible impairment on male fertility. *Asian Journal of Andrology*, **10**(4): 602–606.

Wang JJ, Yu XW, Wu RY, et al. 2018. Starvation during pregnancy impairs fetal oogenesis and folliculogenesis in offspring in the mouse. *Cell Death & Disease*, **9**(5): 452.

Wei Y, Yang CR, Wei YP, et al. 2014. Paternally induced transgenerational inheritance of susceptibility to diabetes in mammals. *Proceedings of the National Academy of Sciences of the United States of America*, **111**(5): 1873–1878.

Weinstein LS, Liu J, Sakamoto A, et al. 2004. Minireview: *GNAS*: normal and abnormal functions. *Endocrinology*, **145**(12): 5459–5464.

Wilson V, Beddington RS. 1996. Cell fate and morphogenetic movement in the late mouse primitive streak. *Mechanisms of Development*, **55**(1): 79–89.

Yan X. 2014. Cognitive impairments at high altitudes and adaptation. *High Altitude Medicine & Biology*, **15**(2): 141–145.

Zhang LB. 2005. Prenatal hypoxia and cardiac programming. *Journal of the Society for Gynecologic Investigation*, **12**(1): 2–13.

Zhang LY, Liu KX, Liu ZQ, et al. 2024a. In pre-clinical study fetal hypoxia caused autophagy and mitochondrial impairment in ovary granulosa cells mitigated by melatonin supplement. *Journal of Advanced Research*, **64**: 15–30.

Zhang LY, Zhang K, Zhao X, et al. 2024b. Fetal hypoxia exposure induces Hif1a activation and autophagy in adult ovarian granulosa cells†. *Biology of Reproduction*, **111**(6): 1220–1234.

Zhang ZM, Luo XF, Lv Y, et al. 2019. Intrauterine growth restriction programs intergenerational transmission of pulmonary arterial hypertension and endothelial dysfunction via sperm epigenetic modifications. *Hypertension*, **74**(5): 1160–1171.

Zhao H, Wong RJ, Stevenson DK. 2021a. The impact of hypoxia in early pregnancy on placental cells. *International Journal of Molecular Sciences*, **22**(18). DOI: 10.3390/ijms22189675

Zhao J, Yao K, Yu H, et al. 2021b. Metabolic remodelling during early mouse embryo development. *Nature Metabolism*, **3**(10): 1372–1384.